Magnetic interactions and electronic states in superconducting and nonsuperconducting ruthenocuprates

Y. Hirai,[1] I. Živkovic,[2] B. H. Frazer,[1,3] A. Reginelli,[3] L. Perfetti,[3] D. Ariosa,[3] G. Margaritondo,[3] M. Prester,[2] D. Drobac,[2] D. T. Jiang,[4] Y. Hu,[5] T. K. Sham,[6] I. Felner,[7] M. Pederson,[8] and M. Onellion[1,*]

[1]*Physics Department, University of Wisconsin, Madison, Wisconsin 53706*

[2]*Institute of Physics, HR-10000 Zagreb, Croatia*

[3]*Institute of Applied Physics, EPFL, CH-1024 Lausanne, Switzerland*

[4]*Canadian Light Source Inc., University of Saskatchewan, Saskatoon, SK, Canada S7N 5C6*

[5]*Canadian Synchrotron Radiation Facility, Stoughton, Wisconsin 53589*

[6]*Department of Chemistry, The University of Western Ontario, London, Ontario, Canada N6A 5B7*

[7]*Racah Institute of Physics, Hebrew University, Jerusalem, Israel*

[8]*Code 6392, Naval Research Laboratory, Washington, DC 20375*

(Received 17 May 2001; published 10 January 2002)

We measured polycrystalline samples of $SrRuO_3$ and both superconducting and nonsuperconducting (hydrogen loaded) ruthenocuprates–$Eu_{1.5}Ce_{0.5}RuSr_2Cu_2O_{10-x}$ (Ru-1222)–samples using ac susceptibility, Ru $3p$ x-ray photoemission and Ru $2p$ x-ray-absorption measurements. The superconducting-and metallic-ruthenocuprate samples exhibit significant ferromagnetic fluctuations above the highest magnetic ordering temperature. The (Ru $3p$) core level of the $SrRuO_3$, and superconducting ruthenocuprate samples indicate that the (Ru) layers are metallic.

DOI: 10.1103/PhysRevB.65.054417 PACS number(s): 75.30.Cr, 75.70.Pa, 75.60.Ej

Recent advances in ruthenate and ruthenocuprate materials have increased interest in the relation between magnetic order and superconductivity in perovskite oxides.[1,2] References 1 and 2 emphasized, in different ways, the significance of ferromagnetic or antiferromagnetic fluctuations in Sr_2RuO_4. Both references note that the (Ru) is in the 4+ valence state and use this valence as part of their arguments. The common issues here are the presence and nature of magnetic fluctuations, and the effects of valence on magnetic and superconducting properties. For the ruthenocuprates,[3–18] there is no consensus yet as to the nature of magnetically ordered state(s) compatible with superconductivity.[12,15–18] There are two main families of ruthenocuprates that have been studied. For $(Eu, Gd)Sr_2RuCu_2O_{8-\delta}$ (Ru-1212) samples, the Curie-Weiss temperature is positive but below the magnetic ordering temperature (T_M), suggesting both ferromagnetic and antiferromagnetic fluctuations in this system.[16] Reference 19 calculated the $(Eu, Gd)Sr_2RuCu_2O_{8-\delta}$ system, concluded that the RuO_2 layers are metallic, that the induced moment on the CuO_2 layers is $\sim 0.01\mu_B$, and argued that one explanation for coexistence of ferromagnetism and superconductivity is a Fulde-Farrel-Larkin-Ovchinnikov[20,21] model. In addition, there is a Ru-1222 family of materials that also includes superconductors. We concentrate on the Ru-1222 materials in this report. For both families of materials, two of the key questions concern (1) the nature of magnetic fluctuations, and (2) whether the RuO_2 layers are metallic.

In this paper, we provide answers to these two questions. Our data lead to the following conclusions.

(i) In contrast to $SrRuO_3$ (and also Ru-1212 samples), the superconducting ruthenocuprate samples (Ru-1222 family) exhibit ferromagnetic fluctuations well above the highest magnetic ordering temperature;

(ii) The (RuO_2) layers of the superconducting ruthenocuprate are themselves metallic at all temperatures, as are the CuO_2 layers.

We found that there was no change in the unoccupied electronic states across the magnetic phase transition, nor any indication in Ru $2p$ magnetic dichroism measurements of long-range ferromagnetic order.

Polycrystalline samples of $SrRuO_3$ and $Eu_{1.5}Ce_{0.5}Sr_2RuCu_2O_{10-\delta}$ were prepared by a solid-state reaction of CeO_2, Eu_2O_3, Ru, and $SrCO_3$. Precursor powders were ground, pressed and then fired at 1000 °C for 24 h in air. The material was then reground, pressed, and fired in 1 atm of O_2, at 1050 °C, for 72 h. We added additional oxygen to a piece of the as-prepared ruthenocuprate sample by placing, it in a swagelok, adding liquid oxygen, sealing the swagelok, and annealing at ~300 °C for 24 h. We added hydrogen by placing a piece of the as-prepared ruthenocuprate sample in a hydrogen-filled vessel, heating to ~280 °C, and cooling back to room temperature over a period of 30 minutes. We characterized the samples using x-ray diffraction and superconducting quantum interference device magnetometry. The measurements reported here include ac susceptibility, x-ray photoemission, and x-ray absorption. The ac susceptibility measurements were taken with a CryoBIND ac susceptometer and used two frequencies, 28.4 and 231 Hz, a 0:7-Oe amplitude ac magnetic field for the lower temperature measurements, and a 20-Oe ac magnetic field for the high-temperature (paramagnetic) measurements. By properly calibrating the ac susceptometer, we were able to express the data in absolute susceptibility units. X-ray photoemission spectroscopy measurements were performed with a Scienta ESCA 300 electron energy analyzer and an Al rotating anode photon source. X-ray-absorption and magnetic circular dichroism measurements were performed at the Wisconsin Synchrotron Radiation Center (SRC) using the Canadian Double Crystal Monochromator and SRC-owned XMCD chamber. The double-crystal monochromator beamline used InSb(111) crystals and the incoming photon flux was moni-

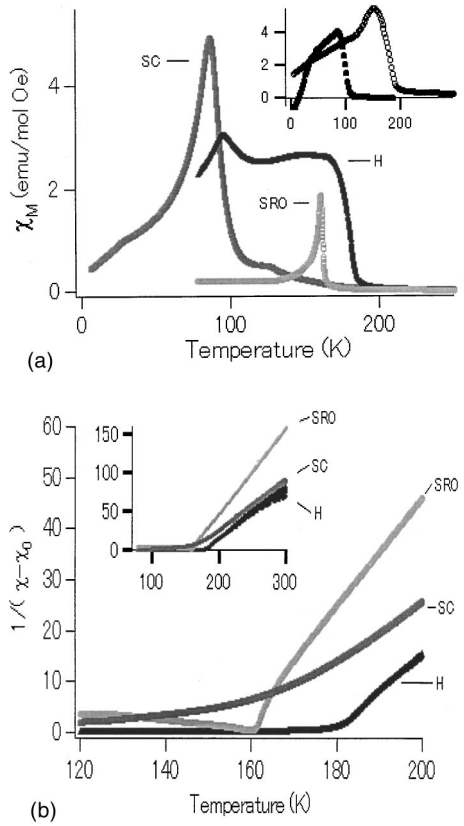

FIG. 1. (a) ac susceptibility data for $SrRuO_3$ (SRO), superconducting ruthenocuprate (SC), and nonsuperconducting (hydrogen-loaded) ruthenocuprate (H) samples. The ac frequency was 23 Hz and the ac magnetic field 0.7 Oe. The vertical axis shows χ_M in units of (emu/mol Oe), and the horizontal axis shows the temperature in K. Inset: dc magnetization vs temperature for superconducting (closed square) and hydrogen-loaded (open square) ruthenocuprates. (b) Inverse susceptibility data for $SrRuO_3$ (SRO), superconducting ruthenocuprate (SC), and nonsuperconducting (hydrogen-loaded) ruthenocuprate (H) samples. Inset: inverse susceptibility in the temperature range 77–300 K. The vertical axis shows $1/(\chi-\chi_0)$ in units of $[\text{emu/mol Oe}]^{-1}$, and the horizontal axis shows the temperature in K. The ac frequency was 28.1 Hz and the ac magnetic field 20 Oe. The data were taken in temperature steps of ~0.1 K, so the data look like solid lines.

tored using an in-line nitrogen ionization chamber. The instrumental energy resolution of the monochromator was ~1 eV.

Figure 1 shows low-field susceptibility data; magnetization data on these samples were previously reported.[3] As illustrated in Fig. 1(a), $SrRuO_3$, the susceptibility line shape in a zero applied dc field is as expected for an itinerant ferromagnet. The superconducting ruthenocuprate exhibits three main responses in susceptibility, magnetic responses at T_{M1} ~120 K and T_{M2}~90 K and, from the inset, DC magnetization data showing a superconducting phase transition at ~30 K. The magnetization data showing superconductivity for as-prepared ruthenocuprates but no diamagnetic-superconducting-response for hydrogen-loaded ruthenocuprates were reported previously.[3] Neither magnetic response exhibits a line shape consistent with a simple ferromagnetic transition. The nonsuperconducting, hydrogen-loaded sample exhibits two visible magnetic responses at T_{M1}~180 K and T_{M2}~90 K; neither line shape is consistent with a simple ferromagnetic response. There is no universal agreement in the literature of the origins of transitions at T_{M1} and T_{M2}. Some of us have suggested that the transitions correspond to changes in the magnetization vector within the RuO_2 planes.[3]

As Fig. 1(b) illustrates, the superconducting (metallic) ruthenocuprate exhibits a Curie-Weiss temperature (Θ) of ~165 K, well above the T_M~122 K. A positive Curie-Weiss temperature indicates ferromagnetic fluctuations, while $\Theta > T_M$ indicates fluctuations and correlations beyond the mean-field approximation. By contrast, both nonsuperconducting samples exhibit Θ that is, within the experimental error of ± 2 K, equal to T_M (157 K for $SrRuO_3$, 180 K for hydrogen-loaded ruthenocuprate); the mean-field approximation applies to these samples.

The data of Fig. 1(b) fit very well to a sum of Curie-Weiss plus constant (Pauli) susceptibility. Using such a fit, we find that the effective moment per (Ru) for $SrRuO_3$ is 2.68 ± 0.01 Bohr magnetons, similar to earlier reports[22–24] of 2.6–2.8 Bohr magnetons. For the superconducting ruthenocuprate Ru-1222, the moment is 3.46 ± 0.05 Bohr magnetons, slightly higher than the 3.14 Bohr magnetons reported for the $RuSr_2(Eu, Gd)Cu_2O_8$ material.[16] For the nonsuperconducting ruthenocuprate, the moment is 2.96 ± 0.05 Bohr magnetons. The superconducting ruthenocuprate value is higher than that expected for purely localized Ru(5+) in the $4d^3 5s^0$ configuration.[25] For $SrRuO_3$ in the $4d^4 5s^0$ configuration, the moment expected would be 0 ($S=2, L=2, J=|L-S|=0$), $4\mu_B$ (L quenched, $J=S=2$, high spin) or $2\mu_B$ (L quenched, $J=S=1$, low spin). None of these corresponds to the measured moment, as expected for an itinerant ferromagnet.

We have measured the ac susceptibility for the samples using ac frequencies from 23 to 800 Hz. We find small changes in the susceptibility with frequency, but no dramatic changes that would, for example, be consistent with classic spin glass behavior.

It is noteworthy to compare the ratio of magnetic moment obtained from paramagnetic data to the saturation moment obtained in the ferromagnetic state. Using the results in the literature for the saturation moment,[3,4,24,26] the ratio is 2.7 ± 0.3 for $SrRuO_3$, 5.1 ± 0.5 for the superconducting ruthenocuprate, and 3.0 ± 0.5 for the nonsuperconducting ruthenocuprate. Using the Rhodes-Wohlfarth criterion,[27,28] the ratio indicates that the magnetization is due primarily to itinerant moments, rather than moments localized to one atomic site, for all samples.

It is important to note that these very low-field results for the Curie-Weiss temperature and the paramagnetic effective magnetic moment differ from results obtained using high magnetic fields. We have confirmed the published data using high magnetic fields, and attribute the difference to the greater response found when using very low applied magnetic fields.

Figure 2 shows Ru $3p$ core level data on both $SrRuO_3$ and superconducting ruthenocuprate samples. We fit the data to three different estimates of the background. It is noteworthy

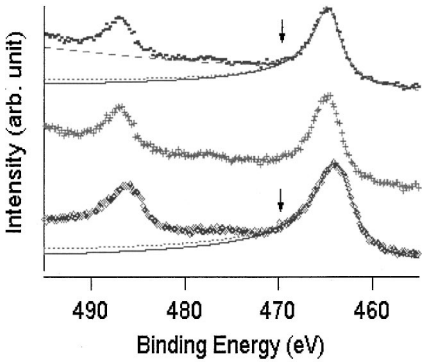

FIG. 2. Ru $3p$ core-level photoemission spectra of superconducting ruthenocuprate samples (top and middle spectra are the same data on the ruthenocuprate) and $SrRuO_3$ (bottom). We provide two copies of the same ruthenocuprate spectrum, with and without fitting, for ease of view by the reader. Also shown are Doniach-Sunjic line-shape fits. We include three fits: (1) Fit to a binding energy of 476 eV (dotted line of the ruthenocuprate samples), which also yields an excellent fit to the background of the entire doublet. (2) Fit based on a constant background and fit to the binding energy emphasized by an arrow (↓) (solid lines). (3) Fit based on a background proportional to the electron binding energy (short dotted lines of both spectra).

that for the same background, we find (within experimental error) the same asymmetry parameter for the superconducting ruthenocuprate and the $SrRuO_3$ data. Using a Doniach-Sunjic[29] analysis, we obtain an asymmetry parameter $\alpha = 0.25 \pm 0.04$. A value of α significantly above zero indicates that the environment around the core photohole is metallic; our data indicate that the RuO_2 planes are almost equally metallic in terms of their electronic response. The value of α is the same between 80 and 300 K, the temperature range over which we obtained data.

Figure 3 illustrates x-ray-absorption data across the Ru $2p$ L_2 and L_3 edges on all four samples. The data in this figure provide information on the unoccupied (Ru) electronic states. Comparison of all data indicate, within the experimental error, that there are no differences in the Ru $2p$ L_2 and L_3 whiteline features (when the peak heights are normalized to unity) and the leading edge locations between 33 and 300 K, the temperature range over which we obtained data. The inflection points on the rising edge are taken as the leading edge. Figure 3(a) illustrates the entire x-ray-absorption spectra for all four samples. Figure 3(b) illustrates the L_2 and L_3 edges. Both edges are shown together to emphasize that the energy separation between the L_2 and L_3 edges is, as expected, the same for all samples. The two metallic ruthenocuprate samples exhibit a leading edge at 1.0 ± 0.3 eV higher photon energy than $SrRuO_3$ or the hydrogen-loaded ruthenocuprate; the latter two exhibit the same leading edge. This is consistent with earlier reports[30] that metallic $Eu_{1.5}Ce_{0.5}Sr_2RuCu_2O_{10-\delta}$ ruthenocuprates exhibit a dominant $(5+)$ valence while the hydrogen-loaded ruthenocuprate exhibits a dominant $(4+)$ valence. Figure 3(c) illustrates the energy-level diagram obtained from the data of Figs. 3(a) and 3(b). Note the 1.0-eV shift of the occupied (both L_3 and L_2) Ru $2p$ states between metallic ruthenocuprate and hydrogen-loaded ruthenocuprate samples. Note that the samples with dominant $5+$ valence exhibit two main transitions,[31,32] while the $4+$ dominant valence samples exhibit one main transition at both edges. We performed magnetic circular dichroism measurements on superconducting (both as-prepared and oxygen annealed) and nonsuperconducting ruthenocuprates at low temperatures (33 K) and found no dichroism signal across the (Ru $2p$) edge. Given the experimental uncertainty, this places an upper limit on possible dichroism signal (absorption intensity difference across L_3 edge between opposite magnetization directions) of 2%.

To interpret our x-ray-absorption spectroscopy (XAS) data, we have calculated spectra by placing a Ru ion inside an oxygen octahedra and adding eight additional alkali atoms (Rb), which leads to a RuO_6Rb_8 cluster. The Ru$(4+)$ valence state corresponds to a d^4 occupancy, while Ru$(5+)$ corresponds to a d^3 occupancy. The results are in good agreement with experiment and are presented in Fig. 4. The neutral and ionized clusters yield Ru $4+$ and Ru $5+$ oxidation states with formal oxygen and alkali charges of -2 and $+4$, respectively. The geometries of these clusters were relaxed for each charge state using NRLMOL which is an all-electron density-functional-based method.[33,34] The Perdew-Burke-Ernzenhof generalized gradient approximation was used for the energy functional.[35] Once the electronic and atomic degrees of freedom were fully relaxed, the L_2 and L_3 spectra were simulated by calculating a dipole-weighted joint density of states between the fully occupied Ru$(2p)$ manifold and the unoccupied states which includes part of the Ru$(4d)$ manifold. This is given by

$$J(E) = \Sigma_{ijx} \langle \Psi_i | x | \Psi_j \rangle^2 F(\lambda_i - \lambda_j - E),$$

with Ψ_i an occupied Ru$(2p)$ wave function, Ψ_j an unoccupied wave function, and $F(\lambda_i - \lambda_j - E)$ a Gaussian-broadening function. The sum over x represents the three spatial dipole operators (x, y, z). The broadening parameter chosen to match the widths of the Ru$(+5)$ data.

Calculations have been performed with and without the spin-orbit operator. The primary effect of the spin-orbit coupling operator is to split the Ru $2p$ states into a quasidoublet and a quasiquartet. The calculated splitting is 121.4 eV, in reasonable agreement with the experimental splitting of the L_2 and L_3 peaks (125 eV). In addition, the quasidoublet and quasiquartet structures exhibit an exchange splitting of approximately 0.25 eV. This splitting is small compared to the $e_g - t_{2g}$ crystal field splitting of the Ru$(4d)$ states which is observed to be 1.0–4.0 eV and is dependent on geometry, charge state and moment.

Figure 4(a) shows the calculated XAS spectra for Ru$(+5)$. The Ru$(+5)$ structure has the majority-spin t_{2g} states fully occupied and the resulting geometry has O_h symmetry. With respect to the occupied majority spin t_{2g} states, the unoccupied majority spin e_g states are 2.4 eV higher in energy, and the unoccupied minority-spin t_{2g} and e_g states are 1.1 and 2.4 eV higher, respectively. Thus a two-peaked structure for the $2p$-$4d$ excitations is observed for Ru$(5+)$. Best agreement between theory and experiment is obtained

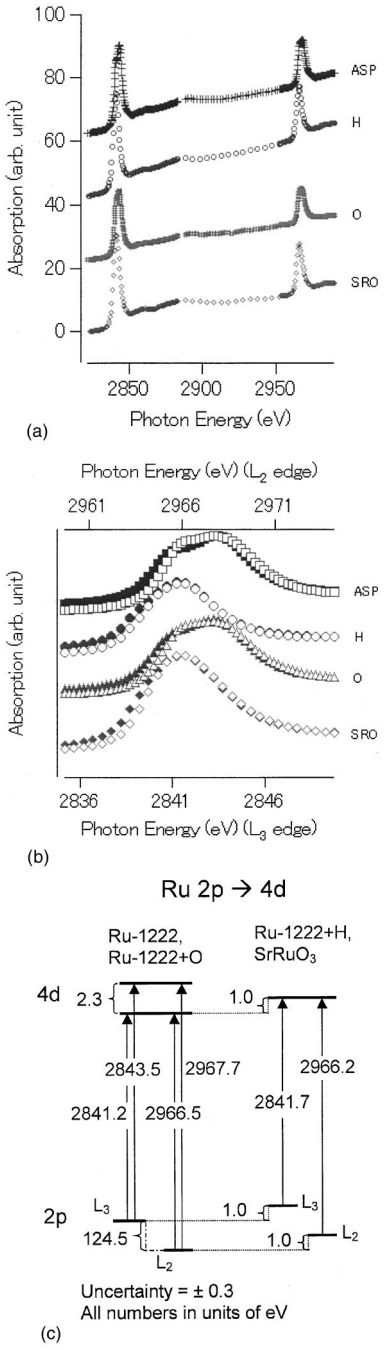

FIG. 3. Ru $2p$ x-ray-absorption spectra for as-prepared Ru-1222 (ASP), nonsuperconducting (hydrogen loaded) Ru-1222 (H), oxygen-annealed Ru-1222 (O), and $SrRuO_3$ (SRO), including (a) full spectra across both the Ru $2p_{1/2}$ and Ru $2p_{3/2}$ edges; (b) expanded view of both edges L_3 (closed symbols) and L_2 (open symbols), aligned by the difference in photon energy between the edges, and (c) energy-level diagram arising from data of (a) and (b). The Ru $2p$ x-ray-absorption spectra were taken with 0.25-eV energy steps. The energy resolution of the monochromator was ~1 eV. The as-prepared and oxygen-annealed ruthenocuprate samples exhibit a 2.3-eV splitting of the unoccupied electronic states that is not present for $SrRuO_3$ or the hydrogen-loaded ruthenocuprate samples.

when a broadening of 2.7-eV is included in the theoretical spectra. The 2.7-eV broadening is reasonable; it is close to the combined effect of instrumentation and lifetime broadening of the Ru $2p$ core hole.[36] There are two disparities between theory and experiment. One is that in Fig. 4(a), the lower photon energy feature is more pronounced, while in Figs. 3(a) and 3(b), the higher photon energy feature is slightly more intense. The other is that the experimental splitting in the ruthenocuprate data of 2.3 eV is larger than the splitting of 1.3 eV ($=2.4\,\mathrm{eV}-1.1\,\mathrm{eV}$) in our calculation. Our calculation is thus in qualitative, but not quantitative, agreement with experiment.

Figure 4(b) shows the calculated XAS spectra for Ru(4+). For Ru(+4) an additional majority spin $4d$ electron is occupied which breaks the O_h symmetry and causes additional splittings (a combination of Jahn-Teller distortions and exchange splittings) of the Ru($4d$) manifold. The effect is to smear out the $4d$ energies leading to the single-peaked structure shown in the figure. The same broadening, 2.7 eV is included in Fig. 4(b) to obtain the best agreement between theory and experiment. We also calculated the spin-resolved density of states for both Ru(5+) and Ru(4+) to confirm that the unoccupied electrons associated with the joint density of states are indeed due to the unoccupied Ru($4d$) manifold. We found that the unoccupied electronic states immediately above the chemical potential are overwhelmingly spin minority, while between 1.0 and 5.0 eV above the chemical potential there is substantial contribution from both spin-majority and minority states.

Figure 2 indicates that the RuO_2 layers for superconducting ruthenocuprates are metallic, as predicted in Ref. 19 This implies that there are metallic layers possessing long-range magnetic order (RuO_2) and superconductivity (CuO_z) for the superconducting ruthenocuprates. As noted in Ref. 19, having both the magnetic and superconducting layers metallic places severe restrictions on how superconductivity and magnetic order can coexist. In particular, when we consider Ref. 16 we note that the (Eu, Gd)$Sr_2RuCu_2O_{8-\delta}$ samples exhibit a Curie-Weiss temperature (Θ): $0<\Theta<T_M$, while the present samples exhibit $0<T_M<\Theta$. These results indicate that superconductivity can coexist with different magnetic fluctuations and relative contribution of ferromagnetic and antiferromagnetic parts of the ordering.

References 16 and 32 argued that, for (Eu, Gd)$Sr_2RuCu_2O_{8-\delta}$ samples, the (Ru) valence is a mixed 4+ and 5+ valent system. The present work does not rule out some admixture of 4+ and 5+ valences, the results merely indicate that for the present superconducting ruthenocuprate samples, the dominant (Ru) valence is 5+. It is also noteworthy that the isostructural compound $Eu_{1.5}Ce_{0.5}Sr_2NbCu_2O_{10-\delta}$ is (a) superconducting, and (b) exhibits no long-range magnetic order.[37–39] As Cava has noted,[40] the Nb layer is expected to be insulating for these superconducting samples. For these samples, Nb is expected to be in the 5+ valence state. The $SrRuO_3$ and Sr_2RuO_4 reference compounds possesses Ru in the 4+ valence state. The first is an itinerant ferromagnet, without superconductivity, while the second is a low-temperature (0.7 K) superconductor. The Ru,Nb system exhibits superconductivity for

both metallic and insulating (RuO_2 or NbO_2) layers. Changing the Ru or Nb layers from insulating to metallic has very little effect on superconductivity, but of course removing carriers from the CuO_2 layers can destroy superconductivity (Fig. 1). These results are consistent with earlier suggestions[9,19] that the CuO_2 and RuO_2 layers are almost completely decoupled.

Figure 3 indicates a difference in valence among the Ru compounds we report on. Further, the dominantly 5+ compounds exhibit two peaks in the unoccupied density of states, while the 4+ compounds exhibit one peak. This is explained theoretically by the results shown in Fig. 4. One unexpected result is a negative one: we measure no change in the Ru unoccupied density of states across the magnetic ordering transition(s). This is in marked contrast with other magnetic systems, for which changes have been reported.[41]

Another surprising result concerns the nature of the magnetic moments in the ruthenocuprates. For $SrRuO_3$ and both superconducting and nonsuperconducting (hydrogen-loaded) ruthenocuprates (Ru-1222,) the Rhodes-Wohlfarth criterion indicates that the magnetism is carried mostly by itinerant moments—that is, moments not localized to one atomic site. Such a result is quite surprising for the nonsuperconducting ruthenocuprates (Ru-1222,) for which dc resistivity measurements indicate a nonmetallic ground state. Previously published O 1*s* XAS data[13] indicated that there is an oxygen pre-edge feature for $SrRuO_3$ and the superconducting ruthenocuprate, as expected for metallic oxides, but no such feature for the hydrogen-loaded ruthenocuprate. The O 1*s* XAS data indicated that in the hydrogen-loaded ruthenocuprate samples, the carriers nearest the chemical potential have little or no oxygen character. We speculate that in the hydrogen-loaded ruthenocuprates, as with the hydrogen-loaded isostructural Nb compound,[37] transport is via hopping. The ratio of 2.7 ± 0.3 for $SrRuO_3$ is consistent with the identification of $SrRuO_3$ as an itinerant ferromagnetic material.

In summary, our data indicate that for the superconducting ruthenocuprate samples reported, the RuO_2 layers are metallic and exhibit ferromagnetic fluctuations above the highest magnetic ordering temperature. Superconductivity coexists with such fluctuations and bulk superconducting phase coherence coexists with metallic magnetically ordered interlayers. Ru is predominantly in the 5+ valence state for superconducting ruthenocuprates, although some 4+ valence cannot be ruled out. The unoccupied electronic states are significantly different for superconducting and nonsuperconducting Ru compounds, and have been successfully modeled by cluster calculations. The calculations show a difference between the Ru(4+) and Ru(5+) spin-resolved densities of states. In the Ru(5+) sample, the splitting of the 4*d* manifold is due entirely to the majority-spin e_g states and minority-spin t_{2g} and e_g states. Because the exchange splitting of the majority and minority spin e_g states is small, a two-peak structure emerges. In contrast, for Ru(4+), a combination of Jahn-Teller distortions and exchange splittings smears out the 4*d* manifold, leading to the appearance of a single-peak structure.

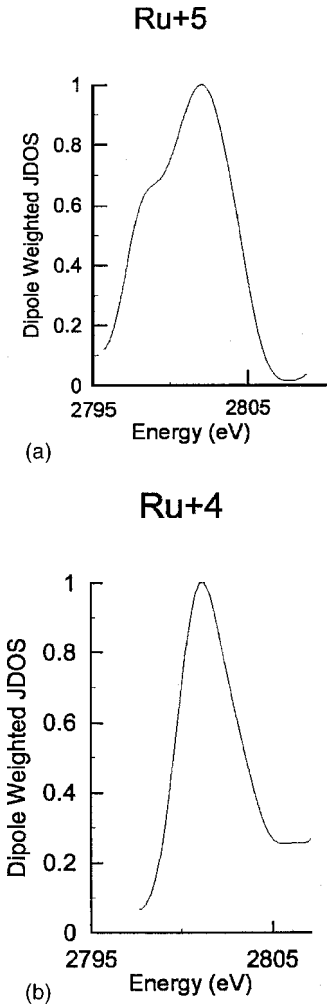

FIG. 4. (a) Theoretical Ru 2*p* x-ray-absorption spectra for a Ru 5+ cluster. (b) Theoretical Ru 2*p* x-ray-absorption spectra for a Ru 4+ cluster. The horizontal axis is the photon energy in eV, while the vertical axis is dipole-weighted joint density of states.

We acknowledge financial support from the Binational Israel USA Foundation BSF (1998), Fonds National Suisse de la Recherche Scientifique, and from the EPFL, NRL, and the National Science Foundation through support of the Synchrotron Radiation Center (Grant No. DMR-0084402).

*Corresponding author.
Email address: onellion@comb.physics.wisc.edu

[1] T. M. Rice, Nature (London) **396**, 627 (1998), and references cited therein.
[2] R. Matzdorf *et al.*, Science **289**, 746 (2000).
[3] I. Felner *et al.*, Phys. Rev. B **55**, R3374 (1997).
[4] I. Felner *et al.*, Phys. Rev. B **57**, 550 (1998).
[5] C. Bernhard *et al.*, Phys. Rev. B **59**, 14 099 (1999).
[6] I. Felner *et al.*, Physica C **311**, 163 (1999).
[7] A. C. McLaughlin *et al.*, Phys. Rev. B **60**, 7512 (1999), and references therein.
[8] A. Fainstein *et al.*, Phys. Rev. B **60**, R12 597 (1999).

[9] I. Felner *et al.*, Physica C **334**, 141 (2000).
[10] J. L. Tallon *et al.*, Phys. Rev. B **61**, R6471 (2000).
[11] C. Bernhard *et al.*, Phys. Rev. B **61**, R14 960 (2000).
[12] J. W. Lynn *et al.*, Phys. Rev. B **61**, R14 964 (2000).
[13] B. H. Frazer *et al.*, Phys. Rev. B **62**, 6716 (2000).
[14] B. H. Frazer *et al.*, Eur. Phys. J. B **19**, 177 (2001).
[15] K. Nakamura *et al.*, Phys. Rev. B **63**, 024507 (2001).
[16] A. Butera *et al.*, Phys. Rev. B **63**, 054442 (2001).
[17] A. Butera *et al.*, J. Appl. Phys. **89**, 7666 (2001).
[18] A. Fainstein *et al.*, Phys. Rev. B **63**, 144505 (2001).
[19] W. E. Pickett *et al.*, Phys. Rev. Lett. **83**, 3713 (1999).
[20] P. Fulde and R. A. Ferrell, Phys. Rev. **135**, A550 (1964).
[21] A. I. Larkin and Yu. N. Ovchinnikov, Zh. Eksp. Teor. Fiz **47**, 1136 (1964) [Sov. Phys. JETP **20**, 762 (1965)].
[22] A. Callaghan, C. W. Moeller, and R. Ward, Inorg. Chem. **5**, 1573 (1966).
[23] J. M. Longo, P. M. Raccah, and J. B. Goodenough, J. Appl. Phys. **39**, 1327 (1968).
[24] G. Cao *et al.*, Phys. Rev. B **56**, 321 (1997).
[25] Specifically this is correct if the orbital angular momentum is quenched. If the orbital angular momentum contributes to the magnetization, then the Lande *g* factor is 1.5 and the moment expected is 2.25 Bohr magnetons/Ru.
[26] J. B. Goodenough, Czech. J. Phys., Sect. B **17**, 304 (1967).
[27] P. Rhodes and E. P. Wohlfarth, Proc. R. Soc. London **273**, 247 (1962).
[28] T. Moriya, *Spin Fluctuations in Itinerant Electron Magnetism*, Springer Series in Solid-State Science Vol. 56 (Springer-Verlag, Berlin, 1985), Sect. 7.1.
[29] S. Doniach and M. Šunjić, J. Phys. C **3**, 285 (1970).
[30] I. Felner *et al.*, Physica B **259**, 703 (1999).
[31] Z. Hu *et al.*, Phys. Rev. B **61**, 5262 (2000).
[32] R. S. Liu *et al.*, Phys. Rev. B **63**, 212507 (2001).
[33] M. R. Pederson and K. A. Jackson, Phys. Rev. B **41**, 7453 (1990).
[34] K. A. Jackson and M. R. Pederson, Phys. Rev. B **42**, 3276 (1991).
[35] J. P. Perdew *et al.*, Phys. Rev. Lett. **77**, 3865 (1990).
[36] *Unoccupied Electronic States*, edited by J. C. Fuggle and J. E. Inglesfield (Springer-Verlag, Berlin, 1992).
[37] Y. Levi *et al.*, Phys. Rev. B **60**, R15 059 (1999).
[38] R. J. Cava *et al.*, Physica C **191**, 237 (1992).
[39] T. J. Goodwin *et al.*, Physica C **204**, 212 (1992).
[40] R. Cava (private communication).
[41] There is a large literature of magnetic circular and linear dichroism measurements on magnetic systems. We used variably polarized light, and measured no magnetic circular or linear dichroism at 33 K, below any magnetic ordering temperature. Note that we performed such magnetic circular dichroism measurements only in remanence.